The Use of InSAR for Monitoring Deformation of Offshore Platforms

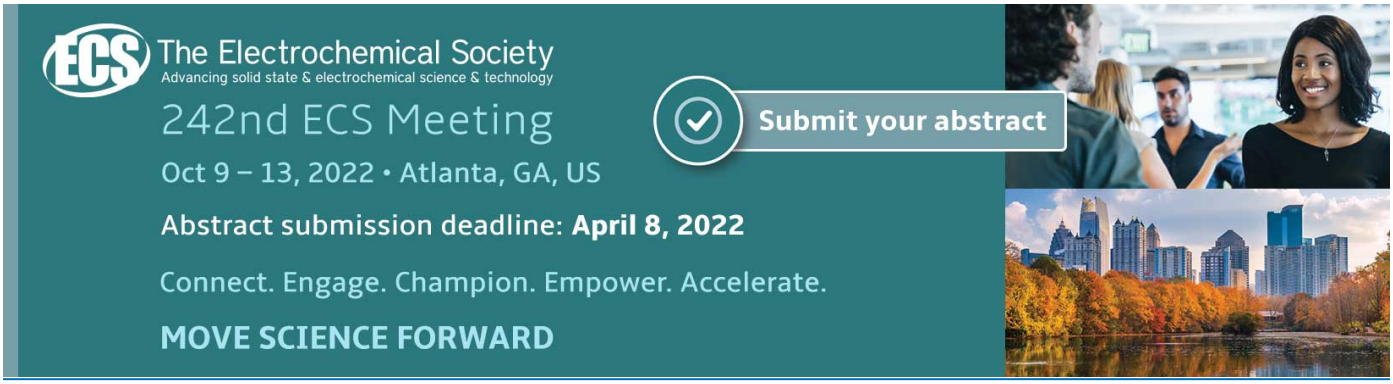

The Use of InSAR for Monitoring Deformation of Offshore Platforms

Amir Sharifuddin Ab Latip[1]*, Abdul-Lateef Balogun[2], Ami Hassan Md Din[3,4] and Andi Mohd Hairy Ansar[3]

[1]Centre of Studies for Surveying Science and Geomatics, Faculty of Architecture, Planning and Surveying, Universiti Teknologi MARA, 40450 Shah Alam, Selangor Darul Ehsan, Malaysia.

[2]Geospatial Analysis and Modelling Research Group (GAMR), Department of Civil and
Environmental Engineering, Universiti Teknologi PETRONAS (UTP), 32610 Seri Iskander, Perak Darul Ridzuan, Malaysia

[3]Geomatics Innovation Research Group (GnG), [4]Geoscience and Digital Earth Centre (INSTEG), Faculty of Built Environment and Surveying, Universiti Teknologi Malaysia, 81310 Johor Bahru, Johor Darul Takzim, Malaysia

amirsharifuddin@uitm.edu.my

Abstract. Fluid extraction or injection from reservoirs, which corresponds to subsidence or uplift, can cause offshore platform surface deformation. Extremely large deformation of offshore platforms often lead to production losses, threat to the structure integrity and loss of life. Therefore, preventing severe deformation incidents is important by monitoring surface deformation caused by oil and gas production activities. In this study, the A1 and B1 offshore platforms have been selected as research study areas to detect surface deformation caused by production activities. A total of 12 radar images from TerraSAR-X satellite were obtained from 24th August 2018 to 22nd August 2019 to derive surface deformation through the Stanford Method for Persistent Scatterers (StaMPS) method. The maximum amounts of subsidence observed on A1 and B1 platforms were -4 mm/yr and -6.3 mm/yr, respectively. This study provides an important insight the use of InSAR technology for the monitoring deformation of offshore platforms.

1. Introduction

Petroleum operations such as the massive exploitation of the fluids (i.e. oil and natural gas) on reservoirs induced structural instability leading to subsidence of the offshore platform [1]. The amount of subsidence depends on many variables, such as the quantity of fluid removed, pore

pressure decline, depth, volume change and overburden. In contrast, uplift of offshore platform occurs depending on the quantity of the fluid injection, pore pressure increase, expansion of the reservoir layer and geological setting (depth, thickness, and area extent). Extreme deformation of offshore platforms may result in loss of life and assets, environmental implications and significant impacts on the image of the industry [2].

The radar interferometry was beginning in the 1970s [3] but it has acted a crucial role in the derivation of the topography of the observed scene and monitoring the displacement on the Earth's surface in the 1980s [4]-[6]. The deployment of several Synthetic Aperture Radar (SAR) satellites into the Earth orbit in the early 1990s had increased the availability of SAR data, making it was more meaningful to detect terrain deformation. The transmitted electromagnetic wave of SAR signal allows the range between the radar sensor and their target on the surface to be measured. DInSAR technique or known as the Differential Interferometric Synthetic Aperture Radar can be used to calculate the phase difference generated from two SAR image observation taken from different time over the same area or the distance shift from the sensor to the target [7]. The phase difference comprises the surface deformation signal and other undesirable phase components induced by topographical, atmospheric and orbital errors. Therefore, it is necessary for extracting the surface deformation signal by removing the phase difference of undesired phase components. However, it is difficult to estimate the deformation signal especially when detecting a small deformation magnitude from a single interferogram when atmospheric noise [8] and de-correlation [9] significantly dominate the deformation signal.

The multi-temporal InSAR or Persistent Scatterer Interferometry (PSI) approaches have been developed to use multiple SAR datasets collected on the same area over a year or years to recognize natural or artificial stable scatter targets (called persistent scatterers (PS) points) in order to resolve the limitation of the DInSAR. This technique eliminates the geometrical and temporal de-correlation impact and effectively minimize error due to atmospheric and improving the deformation measurement [10]- [11]. The first PSI technique was proposed by [12] which called Permanent Scatterers InSAR (PSInSAR). Since then, the ability of the PSI technique has been recognized and further developed by the InSAR research teams and commercial companies. The Stanford Method for Persistent Scatterers (StaMPS) [13], Small Baseline Subset (SBAS) [14], SqueeSAR [15] and Quasi Persistent Scatterers (QPS) [16] are among those of the developed PSI techniques. Each technique uses various approaches, strategies, models or algorithms for processing multiple SAR acquisitions simultaneously. The research conducted by [17] shows that each technique has its own strengths that can retrieve high accuracy of deformation signal (millimetre range) for particular applications (e.g., urban, rural or mountainous regions). A comprehensive review of the different PSI methods has been discussed in [18].

In this paper, the ability of high resolution spaceborne TerraSAR-X data to monitor surface deformation characteristics of the A1 and B1 offshore platforms were discussed. The StaMPS method was used to process the datasets to extract the cumulative surface deformation, deformation rate and displacement time series which provides the deformation history over the analysed PS points.

2. Data acquisition and processing technique

2.1. Study Area and SAR Datasets

In this paper, two offshore platforms (referring to A1 and B1 platforms) were used as monitored platforms. The A1 and B1 platforms are Jacket-Type fixed offshore platforms that serve as production and living accommodation. The two platforms consist of a complex platform (APQ-A/BPQ-A) and an ADR-A/BDR-A satellite platform. The A1 and B1 complexes are within 26 km of

each other.

Twelve TerraSAR-X StripMap images have been successfully acquired for the selected A1 and B1 platforms at 6.47 pm local time on each day of SAR acquisition along the ascending track (from the South to the North). The data were collected in the StripMap mode with the 3-m resolution of images in the same electromagnetic wave polarization mode (horizontally sent - horizontally received (HH)) to ensure a strong response [19]. Each image's size or dimension is 50 km (length) x 30 km (width) at the incidence angle ranges from 43.41º to 45.45º. The images have an acquisition cycle of 33-day starting from 24th August 2018 to 22nd August 2019, for a period of 12 months. The master image (referred to as "M") was chosen near the central point of available dataset to ensure high coherence values obtained over all pairs of scenes. In relation to a common master image obtained on 10th Mac 2019, the maximum perpendicular and temporal baselines of image pairs were 245 meters and 198 days, while the minimum were 7 meters and 33 days. Table 1 presents the perpendicular (***Bperp***) and temporal (***Btemp***) baseline values of the image pairs.

Table 1. Number of images, acquisition dates of the images, baseline values related to the master image.

Number of Image	Acquisition Date (dd/mm/yyyy)	Perpendicular baseline (Bperp) [metres]	Temporal baseline (Btemp) [days]
1	24.08.2018	-19	198
2	26.09.2018	68	165
3	29.10.2018	-93	132
4	01.12.2018	-196	99
5	03.01.2019	172	66
6	05.02.2019	129	33
7	10.03.2019 (M)	0	0
8	12.04.2019	-48	33
9	15.05.2019	-7	66
10	17.06.2019	245	99
11	20.07.2019	-21	132
12	22.08.2019	72	165

2.2. StaMPS Processing Methodology

The StaMPS method was used in this study which developed by [20]. The co-registration was done to match the geometry between the pairs of master and slave images. The MATLAB script was designed to extract high-amplitude pixel coordinates of the master image and computed the offset vectors between master and slave image pairs. By differentiating the radar phase of each pair of slave image and single master image, all sets of interferograms could then be generated. Masking has also been created using MATLAB to remove the undesired region (ocean) around the offshore platform. Then, based on each pixel's amplitude dispersion and phase stability, the Persistent Scatterer Candidates (PSCs) were selected. This approach uses phase characteristic, which was appropriate to find low-amplitude pixels with phase stability that cannot be detected by the existing amplitude-based algorithm.

Immediately after the PS pixels were selected, the deformation signal was isolated from various nuisance terms such as orbital, DEM and atmospheric errors. Unlike the PSInSAR method, a time series of deformation can be produced without require a prior knowledge about the temporal nature of deformation as it can be done by utilizing the spatially correlated nature of the observed deformation phenomena. Moreover, the spatially-uncorrelated look angle error has been subtracted

from the wrapped phase to enhance the precision of the phase unwrapping results. The 3D phase unwrapping algorithm was then carried out to obtain the absolute phase of the selected PS pixels. However, two types of spatially correlated errors still exist in the unwrapped phase: look angle errors and atmospheric errors. The look angle error was determined by high-pass filtering. In the meanwhile, in small area of offshore platforms, the atmospheric error was not supposed to change and therefore, by referring the error to the reference area, it may be cancelled out. The surface deformation was then estimated after reducing all spatially correlated errors from the unwrapped phase. The deformation results included a surface deformation map and a deformation time series over the observed period for each processed PS point. For detailed information on the StaMPS technique can be referred to [21]. The flow chart of the processing from generation of interferogram to deformation estimation is depicted in Figure 1.

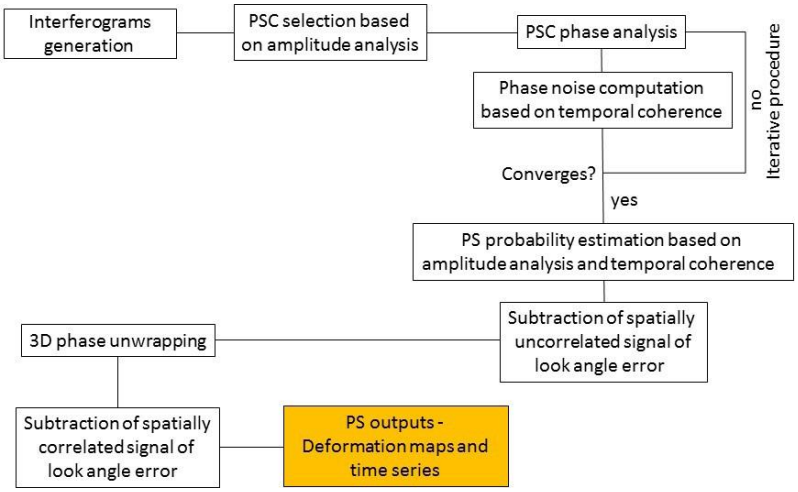

Figure 1. Interferometric processing to estimation of deformation flowchart [24].

3. Results and discussion

3.1. Deformation Analysis of the A1 Platform

Figure 2 displays deformation velocity map of the A1 platform which was calculated from StaMPS during the period between August 2018 and August 2019 (see Table 1). The high density of the PS points / measurement points detected on the A1 platform, which was 151 points. The different colour displayed in PS points represent the average deformation rates range from -4 to 6.8 mm/yr in the line of sight (LOS) direction of the satellite. The warm colours were affected by subsidence (the surface's motion away from the satellite), while cold colours were uplift (the surface's motion toward the satellite). The APQ-A platform experienced with subsidence while the ADR-A platform experienced uplift. Moreover, the bridge connecting between APQ-A and ADR-A did not exhibit any deformation.

Figure 3 indicates the standard deviation of the estimated deformation for A1 platform ranges from 1.1 to 8.5 mm/yr. Thus, the low standard deviation indicates small noises in each measurement. The red colour reflects less error while blue colour reflects high error in computation. Low standard deviation of the estimated subsidence in APQ-A platform shows that the value of the subsidence could be accepted. The deformation time series results were extracted by selecting a PS point and setting the search radius of 20 meters around the selected PS point. Therefore, all the PS points situated inside the

area were also plotted, together with the average of these PS points (see black line) as shown in Figure 4. From the figure, two phases of subsidence can be noticed between the third and fourth data acquisition and the eighth and ninth data acquisition on the APQ-A platform.

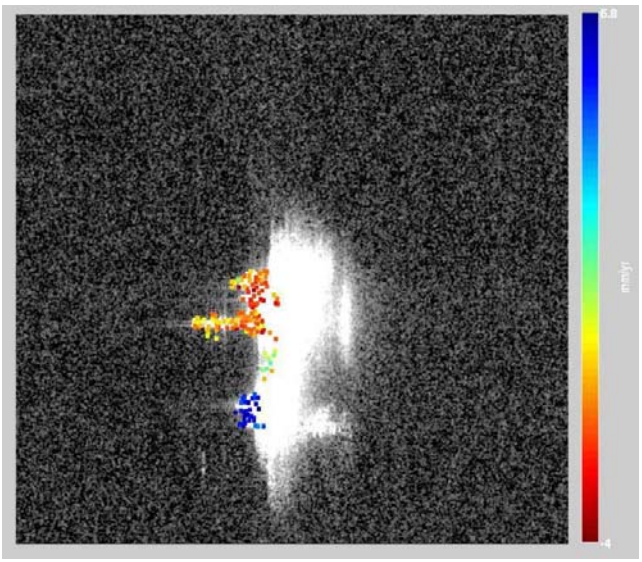

Figure 2. Average rate of deformation at each PS points on the A1 platform.

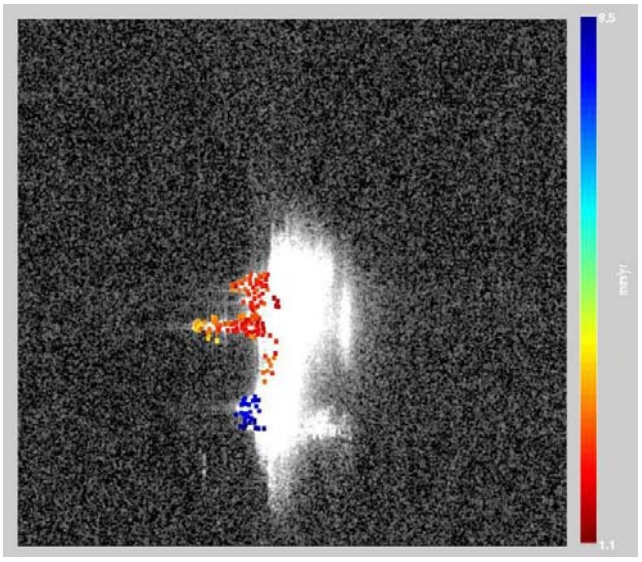

Figure 3. Standard deviation for platform A1 of the estimated deformation.

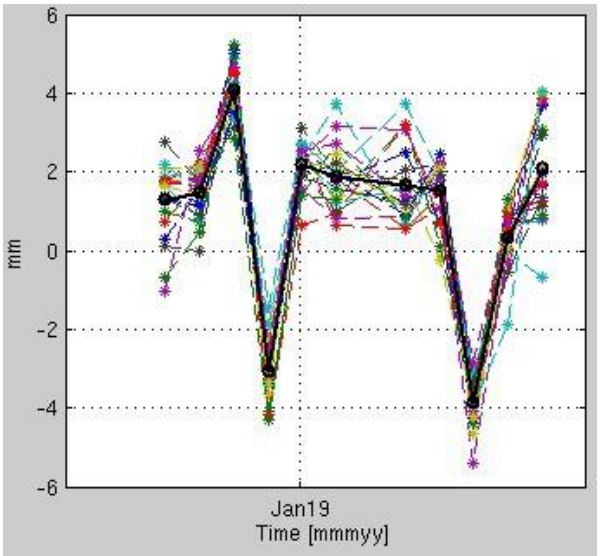

Figure 4. PS points time series analysis located in the subsidence region of the APQ-A platform (each SAR acquisition contains deformation estimates).

3.2. Deformation Analysis on B1 Platform

The spatial distribution of PS points and their corresponding mean displacement rates were revealed in Figure 5. A total of 147 PS points were obtained with an average velocity of deformation ranging from -6.3 to 24.6 mm/yr. The colour coded scale displayed the deformation rates, which green is stable areas, red indicates maximum subsidence areas (-6.3 mm/yr) and blue shows maximum uplift areas (24.6 mm/yr). From Figure 5, subsidence area can be clearly identified at the BPQ-A platform while uplift area at the BDR-A platform. Moreover, the bridge joining between BPQ-A and BDR-A did not show any deformation.

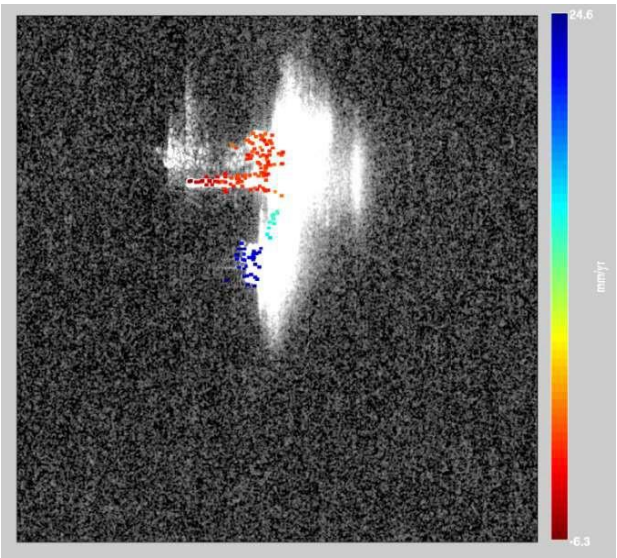

Figure 5. Average deformation for platform B1 of the PS points

The standard deviation has been calculated for the B1 platform to ensure the consistency of the estimated deformation. Figure 6 reveals that, for the B1 platform, the standard deviation of the mean deformation rate was minimal, ranging from 0.2 to 4.1 mm/yr. Figure 7 shows the time series deformation analysis of the PS points selected from the subsidence region or on the BPQ-A platform. The time series reveals that three phases of subsidence could be noticed from the third to fourth, fifth to sixth and seventh to eighth data acquisition.

The A1 platform had subsidence rates of -4 mm/yr and its standard deviation was about 1 mm/yr. Meanwhile, the research found that the subsidence rates of the B1 platform were -6.3 mm/yr with a standard deviation of about 0.2 mm/yr. Since the STD values were low, subsidence was expected to be observed by both platforms. Meanwhile the uplift observed on the offshore platforms could be overlooked and further analysis is needed as the STD values obtained were higher than the observed uplift.

4. Conclusion

The InSAR technique was used to perform the deformation monitoring of the A1 and B1 offshore platforms. This technique has provided remote deformation monitoring without engaging specialist equipment and field operation on the offshore platforms, which effectively minimizing costs, personnel time, logistic operations and site accessibility issues. In this study, the high spatial resolution of the TerraSAR-X image was used because its resolution was adequate for detecting deformation of small structures. Subsidence was observed at the complex platforms (APQ-A and BPQ-A) which the subsidence rate of the B1 complex platform was relatively high compared to the A1 platform. To have access the accuracy of InSAR technique, the GPS derived surface deformation is recommended to be conducted in the future.

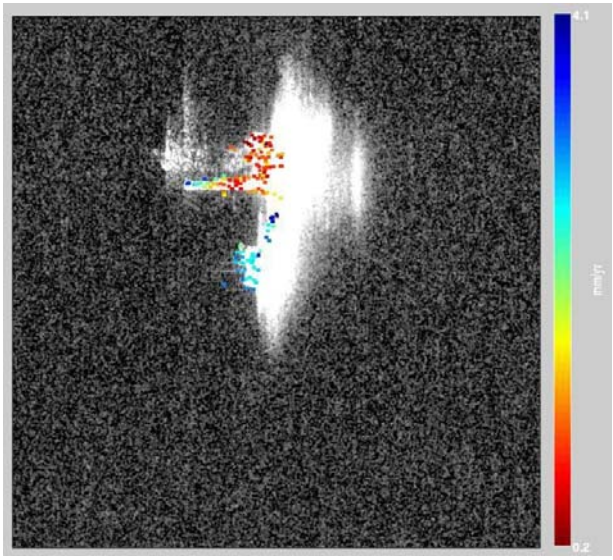

Figure 6. Standard deviation for platform B1 of the estimated deformation.

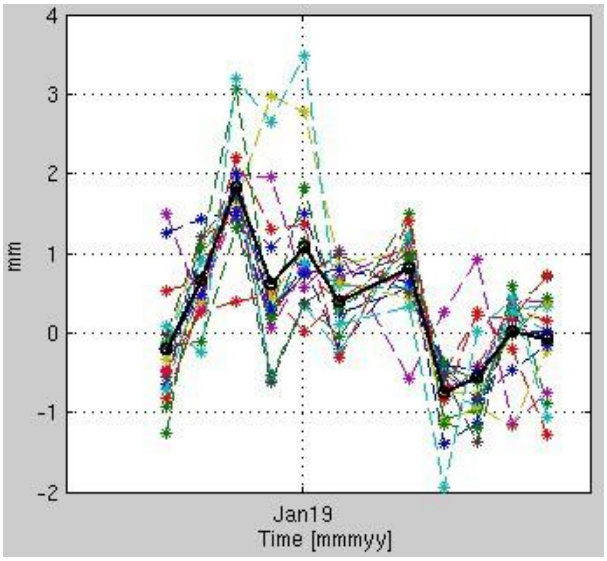

Figure 7. Deformation time series result of PS points situated in the subsidence area of the B1 platform.

References

[1] Kaiser, M.J., 2007. World offshore energy loss statistics. *Energy Policy*, 35(6): 3496-3525.

[2] Latip, A.S.A., Matori, A., Aobpaet, A. and Din, A.H.M., 2015. Monitoring of offshore platform deformation with stanford method of Persistent Scatterer (StaMPS), 2015. *International Conference on Space Science and Communication, IconSpace*, 2015-September, pp. 79–83, 7283785.

[3] Graham, L.C., 1974. Synthetic interferometer radar for topographic mapping. *Proceedings of the IEEE*, 62(6): 763-768.

[4] Gabriel, A.K., Goldstein, R.M. and Zebker, H.A., 1989. Mapping small elevation changes over large areas: differential radar interferometry. *Journal of Geophysical Research: Solid Earth*, 94(B7): 9183-9191.

[5] Goldstein, R.M., Zebker, H.A. and Werner, C.L., 1988. Satellite radar interferometry: Two-dimensional phase unwrapping. *Radio science*, 23(4): 713-720.

[6] Zebker, H.A. and Goldstein, R.M., 1986. Topographic mapping from interferometric synthetic aperture radar observations. *Journal of Geophysical Research: Solid Earth*, 91(B5): 4993- 4999.

[7] Bamler, R. and Hartl, P., 1998. Synthetic aperture radar interferometry. Inverse problems, 14(4): R1.

[8] Zebker, H.A., Rosen, P.A. and Hensley, S., 1997. Atmospheric effects in interferometric synthetic aperture radar surface deformation and topographic maps. *Journal of Geophysical Research: Solid Earth*, 102(B4): 7547-7563.

[9] Zebker, H.A. and Villasenor, J., 1992. Decorrelation in interferometric radar echoes. *IEEE Transactions on geoscience and remote sensing*, 30(5): 950-959.

[10] Md Din, A.H., Md Reba, M.N., Omar, K.M., Ses, S., Ab Latip, A.S., 2015. Monitoring vertical land motion in Malaysia using Global Positioning System (GPS), in: *ACRS 2015 – 36th Asian Conference on Remote Sensing: Fostering Resilient Growth in Asia, Proceedings.*

[11] Din, A.H.M., Zulkifli, N.A., Hamden, M.H. and Aris, W.A.W., 2019. Sea level trend over Malaysian seas from multi-mission satellite altimetry and vertical land motion corrected tidal data. *Advances in Space Research*, 63(11): 3452-3472.
[12] Ferretti, A., Prati, C. and Rocca, F., 2000. Nonlinear subsidence rate estimation using permanent scatterers in differential SAR interferometry. *IEEE Transactions on Geoscience and Remote Sensing*, 38(5): 2202-2212.
[13] Hooper, A., 2008. A multi-temporal InSAR method incorporating both persistent scatterer and small baseline approaches. *Geophysical Research Letters*, 35(16).
[14] Berardino, P., Fornaro, G., Lanari, R. and Sansosti, E., 2002. A new algorithm for surface deformation monitoring based on small baseline differential SAR interferograms. *IEEE Transactions on Geoscience and Remote Sensing*, 40(11): 2375-2383.
[15] Ferretti, A., Fumagalli, A., Novali, F., Prati, C., Rocca, F. and Rucci, A., 2011. A new algorithm for processing interferometric data-stacks: SqueeSAR. *IEEE Transactions on Geoscience and Remote Sensing*, 49(9): 3460-3470.
[16] Perissin, D. and Wang, T., 2012. Repeat-pass SAR interferometry with partially coherent targets. *IEEE Transactions on Geoscience and Remote Sensing*, 50(1): 271-280.
[17] Osmanoğlu, B., Sunar, F., Wdowinski, S. and Cabral-Cano, E., 2016. Time series analysis of InSAR data: Methods and trends. *ISPRS Journal of Photogrammetry and Remote Sensing*, 115: 90-102.
[18] Crosetto, M., Monserrat, O., Cuevas-González, M., Devanthéry, N. and Crippa, B., 2016. Persistent scatterer interferometry: A review. *ISPRS Journal of Photogrammetry and Remote Sensing*, 115: 78-89.
[19] Lazecký, M., 2011. Monitoring of terrain relief changes using Synthetic Aperture Radar Interferometry: Application of SAR Interferometry Techniques in a specific undermined Ostrava-Karviná district, PhD thesis, Ostrava: VSB-TUO.
[20] Hooper, A., Segall, P. and Zebker, H., 2007. Persistent scatterer interferometric synthetic aperture radar for crustal deformation analysis, with application to Volcán Alcedo, Galápagos. *Journal of Geophysical Research: Solid Earth*, 112(B7).
[21] Latip, A.S.A., Matori, A.N. and Aobpaet, A., 2018. A Case Study on Offshore Platform Deformation Monitoring by using InSAR, MATEC Web of Conferences. EDP Sciences, pp. 04002.

Acknowledgements
This research was funded by the Yayasan University Teknologi Petronas (YUTP-FRG) (0153AA-H15).